Alexey Eremin*, Hajnalka Nádasi and Ralf Stannarius*

Multifunctionality by dispersion of magnetic nanoparticles in anisotropic matrices

Abstract: Interactions between magnetic nanoparticles and an anisotropic environment give rise to a variety of new magneto-optical, rheological and mechanical phenomena. This opens new avenues for developing novel multifunctional materials. In the course of this project, we investigated three types of anisotropic systems: dispersions of shape-anisotropic nanocrystals, magnetically doped molecular and colloidal liquid crystals, and organoferrogels. They were investigated by means of magneto-optical observations and by a magneto-mechanical torsion pendulum method.

Keywords: magnetic gels, magnetic suspensions, liquid crystals

1 Aims and concepts

Magnetic fluids are composed of nanometre- to micrometre-sized solid particles in a liquid carrier. A combination of the magnetic properties of the dispersed particles with the fluidity of the matrix enables the development of broadly applicable magneto-responsive materials. In these fluids, interactions with external magnetic fields occur with the individual magnetic particles (MPs). Thus, the interaction energies are not large with respect to thermal energies, in contrast to magnetic solids of the same material as the MPs. In the absence of external magnetic fields, ferrofluids lack a remanent magnetization, they behave like superparamagnets. Confining the magnetic liquid phase in a viscoelastic environment by gelation brings about mechanical and diffusive constraints resulting in materials with distinct sensitivity to mechanical stress and/or magnetic field.

Liquid-crystalline phases are characterized by spontaneous collective orientational order of the molecules in certain temperature or concentration ranges. However, the common liquid crystal (LC) mesogens are diamagnetic, and their interactions with magnetic fields in the mesophases are governed by the anisotropy of the diamagnetic susceptibility of the order of 10^{-6}. The collective arrangement of the mesogens allows us to switch their preferential direction, the director $\vec{n}$, even in weak magnetic fields of

***Corresponding authors: Corresponding author: Alexey Eremin**, Otto von Guericke University, Institute of Physics, Magdeburg, Germany, E-mail: alexey.eremin@ovgu.de; and **Ralf Stannarius**, Otto von Guericke University, Institute of Physics, Magdeburg, Germany, E-mail: ralf.stannarius@ovgu.de
Hajnalka Nádasi, Otto von Guericke University, Institute of Physics, Magdeburg, Germany

https://doi.org/10.1515/psr-2019-0111

a few hundreds mT. This allows to employ magnetic fields for magneto-optical or magnetomechanical switching even without MNPs.

It is a promising but also challenging concept to combine these two areas of soft-matter physics, magnetic fluids and LCs, to create new classes of multifunctional materials that combine a strong magnetic response with collective magneto-optical and magnetomechanical effects. A promising strategy is the dispersion of functionalized MNPs in anisotropic environment such as suspensions of shape-anisotropic (anisometric) microparticles, lyotropic nematic matrices or even thermotropic LCs. We describe how interactions of MNPs with complex anisotropic matrices drive self-assembly and affects the physical properties of the materials. Primary focus is the influence of the matrix structure on the magneto-optical and viscoelastic properties of the composites. An external magnetic field triggers self-organization of the MNPs, which affects the anisotropic environment (matrix). The feedback of the matrix determines the structure formation dynamics of the magnetic subphase, as well as optical and mechanical properties. We examine three different matrix systems: non-MPs (pigment crystallites) dispersed in an isotropic liquid, organic LCs, and organogels with filamentary internal structure. A special aspect is the transition from isotropic to anisotropic matrices.

The following section discusses mixtures of magnetic nanoparticles with shape-anisotropic (rod-like and plate-like) nanocrystallites in suspension. These suspensions may form lyotropic phases at larger particle concentrations, but even at low concentrations the steric interactions with codispersed MNPs enhance the macroscopic response to magnetic fields considerably. The idea is to exploit these interactions to command the larger nonmagnetic constituents via magnetic torques of external fields on MNPs and agglomerations of the latter. In Section 3, we briefly describe attempts to suspend surface-functionalized MNPs in thermotropic nematic LCs. Here, the mesogens are thermodynamically stable LC mesophases. The surface-functionalized MNPs interact with the director field to transfer magnetic alignment to the nematic host. In Section 4, the complexity is increased by physical cross-linking of the host phase. This leads to self-organized arrangements of the MNPs in the gel matrix and to the dependence of mechanical and optical sample parameters on the magnetic history of the material.

In the final section, we introduce a mechanical characterization technique that can be employed to all of these systems. It can be used to characterize magnetomechanical properties of the fluids, in particular the transfer of torques from the magnetic field to the carrier fluid and sample containers.

2 Colloidal suspensions of anisometric particles

Colloidal suspensions of anisometric nanoparticles particles are scientifically attractive because of their ability to form microstructured and nanostructured phases [1–6].

Phases with broken rotational (nematics) and translational (smectics, columnar) symmetries have been discovered in various colloidal materials including clay [7–9], goethite [10, 11], TiO_2 rods [12], viruses [13–16], or even microparticles. Due to a coupling between the orientational degrees of freedom and external fields, these dispersions show a complex rheological response and a distinctive behaviour in electric fields [4, 17].

The crucial role of entropy-driven self-assembly in the colloidal systems is particularly pronounced in binary mixtures of rod-shaped or platelet-shaped nonmagnetic nanoparticles (NPs) with MNPs [18]. These mixtures exhibit a sterically-induced orientation transfer (Onsager-Lekkerkerker effect) [18, 19]. A field-induced alignment of the MNP subsystem is transferred to the nonmagnetic components. This does not only work with shape-anisotropic MNPs. A uniform external magnetic field can cause the formation of small, stable clusters of spherical MNPs which, in turn, may command the orientation of the nonmagnetic constituents.

One example of the sterical orientation transfer occurs in dispersions of rod-shaped pigment nanocrystallites doped with MNPs. Pigment particles investigated in our study (C.I. Pigment Red) have an average length of 230 ± 70 nm and a diameter of 46 ± 20 nm [20]. The particles form a stable dispersion in dodecane with the commercially available dispersant Solsperse 11200 (Lubrizol, Brussels, Belgium). The magnetic dopant is a commercially available ferrofluid (APG 935, Ferrotec), containing magnetite NPs with an average diameter of about 10 nm suspended in hydrocarbons. In our study, we investigated dispersions with various concentrations of MNPs, as well as pigment nanorods (NRs).

2.1 Magneto-optical behaviour

The orientational order of the pigment NRs determines the birefringence of the dispersions, which was measured using the optical modulation technique [21]. Diluted dispersions of the ferrofluid exhibit only weak birefringence saturating above 200 mT. Dispersions of pigment NRs show even weaker magneto-optical response compared to the magnetic fluid. The alignment of the pigment NRs was demonstrated by measurements of the linear dichroism in strong magnetic fields [22]. The particles align perpendicular to the field direction in fields of about 5 T.

By contrast, mixtures of the pigment NRs and MNPs exhibit much higher birefringence in comparison to that of the pigment-only suspensions, where the birefringence is nearly zero, and also in comparison to that of pure MPs. Figure 1 shows the birefringence of the NR/MNP mixtures with pigment particle concentration $c_r = 5$ vol% and varying concentration of MNPs (c_s). The curves exhibit a saturating at about 200–300 mT, which is comparable to that of the ferrofluid. Nevertheless, the birefringence is strongly enhanced by the presence of the NRs. The maximum birefringence Δn_{max} attained at 640 mT is shown in Figure 2.

At a constant c_s and low NR concentrations, the birefringence increases linearly, while for high c_r, a different behaviour is observed (Figure 2). This dramatic increment of birefringence can be explained by an onset of an orientationally ordered phase of the pigment suspensions at high concentrations. At the same time, the maximum birefringence at a constant c_r shows a linear dependence on c_s (see Figure 2) in the investigated concentration range.

2.2 Sterical orientation transfer

The sterical orientation transfer can be described by considering the free energy expansion for a binary mixture of nonmagnetic colloidal rods and magnetic rods. In a mixture of N_1 magnetic and N_2 nonmagnetic rods ($N = N_1 + N_2$) with corresponding lengths and diameters L_1, D_1 and L_2, D_2, respectively, the free energy expansion can be given by [23, 24]:

$$\frac{\Delta F}{Nk_BT} = \frac{\mu^0}{k_BT} - 1 + \ln c + (1-x)\ln(1-x) + x\ln x + (1-x)\sigma_1 + x\sigma_2 + c$$
$$\left[b_{11}(1-x)^2\rho_{11} + 2b_{12}x(1-x)\rho_{12} + b_{22}x^2\rho_{22} \right] - ax \int \cos\beta f_2(\Omega)\, d\Omega \qquad (1)$$

where μ^0 is the chemical potential, c is the net number density of all particles, x is the fraction the magnetic rods of the total number of rods, $(1–x)$ is the fraction of nonmagnetic rods, $a = (\mu H)/(k_bT)$, $b_{ij} = \frac{\pi}{8}(D_i + D_j)L_iL_j$, and β is the angle between **H** and

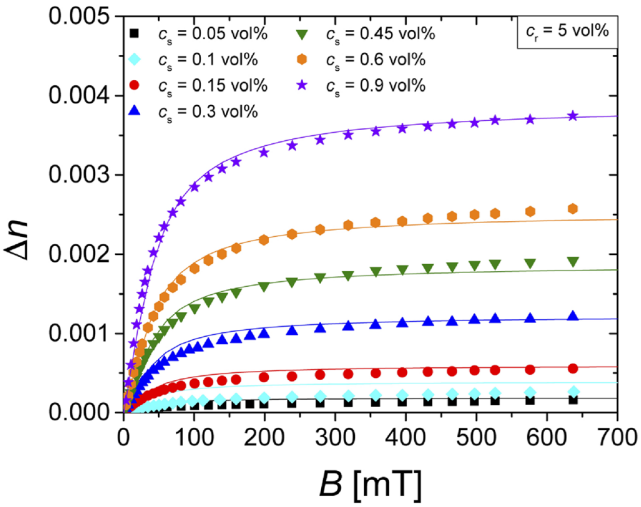

Figure 1: Birefringence of mixtures with pigment particle concentration c_r = 5 vol% and varying MPs concentration (c_s). (Adopted from a study by May et al. [21]).

$\boldsymbol{\mu}$ (i.e. the magnetic moment of the magnetized rods). The integration is over the solid angle Ω describing the orientation of the particles.

$$\sigma_i = \int f_i(\Omega) \ln 4\pi f_j(\Omega)\, d\Omega, i = 1,2 \tag{2}$$

and

$$\rho_{ij} = \iint |\sin\gamma| f_i(\Omega_i) f_j(\Omega_j)\, d\Omega\, d\Omega', i,j = 1,2 \tag{3}$$

where γ is the angle between two vectors defined by the angles Ω and Ω′, $f_1(\Omega)$ and $f_2(\Omega)$ are normalized distribution functions of the two particle types.

For the calculations, it is assumed that both particle types are monodispersed and the chains of MPs are treated as magnetic rods with the lengths of two spherical particles and the widths of one. Thus, the MPs are approximated as short cylinders 28×14 nm in size and with the magnetic moments of two spherical MPs. The calculated distribution function determines the orientational order parameters S_i (i = s,r) of both particle types:

$$S_i = \int \frac{1}{2} f_i (3\cos^2\theta - 1)\, d\Omega, \tag{4}$$

with θ being the angle between the long axis of a rod and the director. The resulting birefringence is

$$\Delta n = \Delta n_{0,\mathrm{r}}\, c_\mathrm{r}\, S_\mathrm{r} + \Delta n_{0,\mathrm{s}}\, c_\mathrm{s}\, S_\mathrm{m}. \tag{5}$$

where $\Delta n_{0,\mathrm{s}}$ and $\Delta n_{0,\mathrm{r}}$ are specific birefringences of the magnetic and rod-shaped particles, respectively. As expected, the measured birefringence and calculated order parameters for constant concentrations are approximately proportional to each other. The birefringence curves $\Delta n(B)$ could be fitted well with Eq. (5) containing numerically estimated order parameters S_r and S_s and the specific birefringence $\Delta n_{0,\mathrm{r}} = 0.7$. The numerical results fit the experimental data well; in particular, the behaviour of the maximum birefringence at constant pigment particle concentration shows good agreement. In contrast, the maximum birefringence at high c_r deviates from the numerical results. This behaviour is a consequence of polydispersity, which leads to a decreased transition concentration to the nematic phase [19].

2.3 Molecular dynamics simulation

The molecular dynamics (MD) simulations were performed by Stavros D. Peroukidis and Sabine H. L. Klapp at the TU Berlin [21]. The model fluid consisted of a binary mixture of N_r uniaxial rods and N_s magnetic spheres. The rods were represented as prolate, nonmagnetic ellipsoids with a length l and the width σ_0 (l/σ_0=3) that interact via the Gay-Berne (GB) potential, using a standard parametrization [21]. The magnetic spheres are modelled via dipolar soft spheres (DSSs), with an embedded central dipole

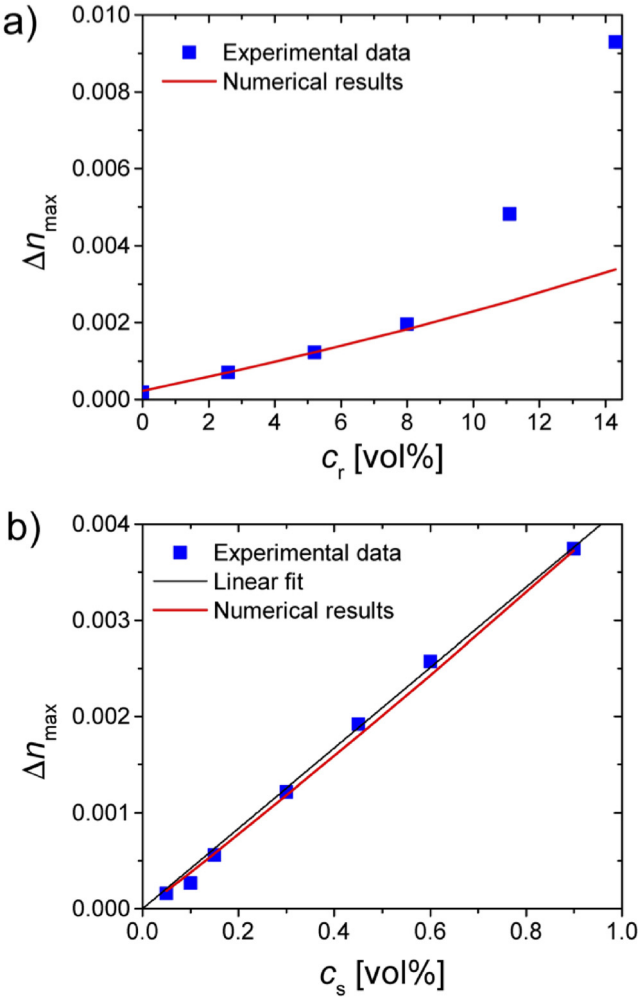

Figure 2: Saturation birefringence: (a) at a constant magnetic particle concentration of $c_s = 0.3$ vol% and different pigment particle concentrations c_r, and (b) at constant pigment particle concentration $c_r = 5$ vol% and different MNP concentrations c_s. (Adopted from a study by May et al. [21]).

moment $\boldsymbol{\mu}$. They interact via a soft repulsive potential and a dipole-dipole interaction [25, 26]. The DSS particles have a diameter σ_s which was set to 1/4 the width of the rods, i.e. $\sigma_s^* = \sigma_s/\sigma_0 = 0.25$, which is consistent with the estimated relative sizes of the experimental species.

In the simulation, GB/DSS mixtures were studied in a uniform magnetic field H at various field strengths $H^* = \mu H/k_B T$, where μ is the dipole moment of a particle. The reduced density is defined as $\rho^* = N\sigma_0^3/V$ and V is the volume of the system with $(N = N_s + N_r)$, fraction of particles $x_a = N_a/N$ (where a = r,s for rods and spheres,

respectively). Five states were considered: $[(\rho^*,x_s) = (0.350,0.20)]$, $[(\rho^*,x_s) = (0.560,0.50)]$, $[(\rho^*,x_s) = (0.778,0.64)]$, $[(\rho^*,x_s) = (1.00,0.72)]$, and $[(\rho^*,x_s) = (1.40,0.80)]$,, that correspond to the isotropic phase of a field-free GB-DSS mixture. For these states the concentration of rods was kept the same (c_r = 44 %) whereas the concentration of DSS, c_s, was varied (it increases by increasing the concentration x_s).

Figure 3 shows the calculated order parameter $S^{(r)}$ and the magnetization $\langle M \rangle$ as functions of the magnetic field. Both magnetization and order parameter exhibit saturating behaviour. The saturation order parameter $S_{saturation}$ has a linear dependence on the concentration of the magnetic spheres as shown in Figure 4. Since the birefringence is proportional to $S^{(r)}$, the result in Figure 4 demonstrates a qualitative agreement between the theory and the experiment. The simulations also show that the optical response of the binary mixtures is expected to decrease if the magnetic interactions between the spheres are reduced. Therefore, not only the concentrations of the MPs but also the interparticle interactions determine the response of the binary systems to an external magnetic field.

3 Dispersions of magnetic NPs in a nematic LC

Dispersions of MNPs in a nematic LC are called ferronematics (FN). We investigated the coupling between the nematic director and the magnetic order of $CoFe_2O_4$-based functionalized MNPs, which were synthesized in the group of Silke Behrens (KIT) [27]. The particle size was around 2.5 nm. In the MNP-doped system, a significant decrease of the magnetic Fréedericksz threshold was found. This suggested the existence of the coupling between the nematic director and the magnetization of small clusters of the MNPs in a particular manner. The MNP clusters represent inclusions in the director field that distort the surrounding director field. The behaviour of the LC dispersions was described using the Raikher-Burylov (RB) model for some of these systems and estimated the magnetization-director coupling strength [27].

At a combined application of electric and magnetic fields to a nematic LC in a planar sandwich cell, one can increase the electric Fréedericksz threshold field by choosing the direction of the magnetic field perpendicular to the electric field, in the cell plane. In absence of MNP doping, the diamagnetic torque on the director stabilizes the ground state. The addition of MNPs reverses this effect, the MNP aggregates align with the magnetic field and destabilize the director ground state. The details of these experiments are found in the contribution by S. Behrens et al. in this volume.

4 Mobile magnetic NPs in fibrillous gels

Ferrogels are composite materials consisting of MPs embedded in a viscoelastic matrix [28]. Their magnetoelastic properties enable applications in the fields of transducers,

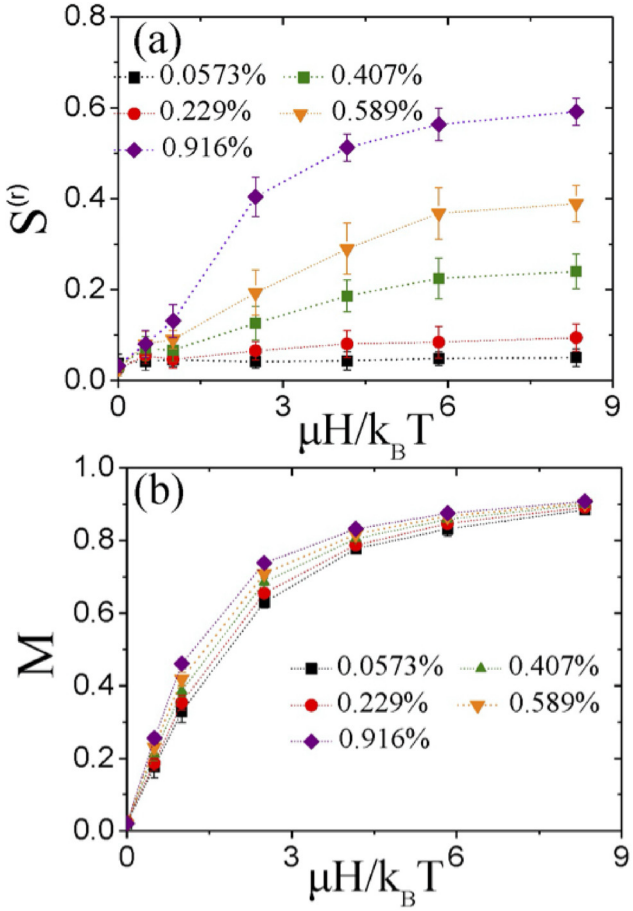

Figure 3: (a) Nematic order parameter of the rod species $S^{(r)}$ and (b) magnetization $\langle M \rangle$ of the MPs as a function of the external magnetic field strength for a GB-DSS mixture with reduced magnetic dipole moment $\mu^* = 2.4$ of the MNPs. The results are taken for constant concentration of rods $c_r = 44$ % by varying the concentration of magnetic spheres c_s. (Adopted from a study by May et al. [21]).

sensors and actuators [29]. Depending on the viscoelastic properties of the matrix, the magnetic properties of the particles and the strength of the coupling between them, their response to external stimuli like, e.g. magnetic fields or mechanical stress can be tuned in a wide range [30, 31]. Especially strong magnetomechanical response is expected when the MPs are micronsized and connected to the viscoelastic matrix. In this case the viscoelastic matrix directly experiences the torque of the Brownian rotation exhibited by the MPs when they align to the applied magnetic field [28]. On the other hand, a strong magneto-optical response can be expected from ferrogels where the MPs are not connected to the matrix and their alignment and chain formation along the

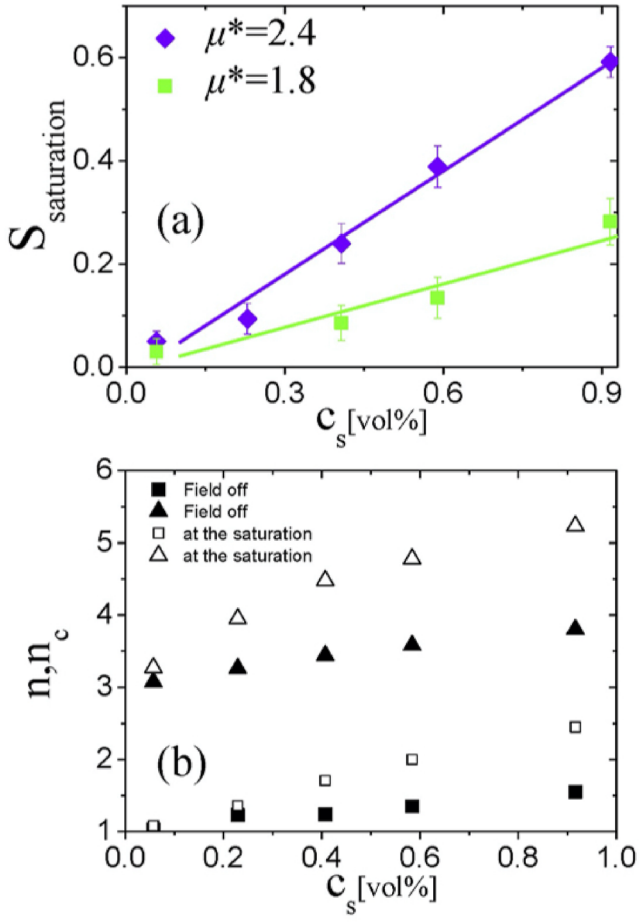

Figure 4: (a) Saturation value of the nematic order parameter of rods $S^{(r)}$ as a function of c_s for constant $c_r = 44$ %, and various values of dipolar moment μ^*. (b) Mean size (number of particles) of all clusters $\langle n \rangle$ -open squares- (irrespective of their type) and mean size of chainlike clusters $\langle n_c \rangle$ -open triangles- at the saturation value of $S^{(r)}$. The corresponding values of $\langle n \rangle$ and $\langle n_c \rangle$ when the field is off are shown by solid squares and triangles, respectively. (Adopted from a study by May et al. [21]).

magnetic field is only determined by the void accessibility in the confined volume of cavities in the mesh [32–36].

The ferrogels prepared in our laboratory belong to the latter category [37]. They consist of commercially available APG2135 ferrofluid diluted with n-dodecane and gelled by 12-hydroxyoctadecanoic acid (12-HOA) gelator. APG2135 consists of single-domain superparamagnetic magnetite particles surrounded by a surfactant layer to avoid aggregation and suspended in a synthetic hydrocarbon carrier. The average core diameter of the particles is 10 nm. The saturation magnetization is 17885 A m^{-1} and the

volume fraction of the particles is 3.9 vol%. The particle size distribution can be described by a lognormal distribution with an average hydrodynamic diameter of D_0 = 14.5 nm and a standard deviation σ = 1.2 [38, 39]. Diluting APG2135 with the nonpolar solvent n-dodecane results in stable suspensions. The initial birefringence of those ferrofluids is insignificant and indicates the presence of some aggregates in the ferrofluid. The origin of birefringence in magnetic fluids can be explained in the following way. In a magnetic field, the MNPs are equivalents of magnetic dipoles aligning along the field in head-to-tail fashion. In the electric field of linearly polarized light they become oscillating dipoles. Depending on the orientation of the chains with respect to the direction of the polarization of the light, the oscillating dipole interaction between the particles is asymmetric, resulting in a strong optical anisotropy. Thus, the birefringence of the ferrofluid increases with increasing magnetic field [40–48]. The maximum birefringence at a given field strength is only dependent on the concentration of the MPs, as can be seen in Figure 7a.

Gelling the ferrofluids brings about several constraints into the system. Since the gelator network divides the volume into cavities with certain amounts of MNPs, there is a limited amount of available particles to form chains. Additionally, due to adsorption along the cavity walls MNPs become immobilized depleting the MNP supply. As a result there will be a smaller number of MPs available in the vicinity of a given particle to form chains than in a ferrofluid.

The mobilities of single particles will be heterogenous and spatially dependent because the alignment of chains along the magnetic field is restricted by the restrained void accessibility. The translational degree of freedom of the particles is constrained by the cavity walls leading to imperfect alignment of the dipoles in the confined space. The torque exhibited by the translations and rotations of the MNPs and their aggregates leads to a deformation of the gel network. These irreversible (inelastic) deformations happen when the ferrogel is exposed to a magnetic field for the first time [49] (Figure 5).

The gelator network is formed by 12-hydroxyoctadecanoic acid (12-HOA) molecules. This chiral low-molecular-weight gelator [50–53] crystallises in organic solvents and due to the anisotropy of strong intermolecular interactions between the individual gelator molecules gives rise to a helical self-assembly in one dimension. The anisotropy of the interfacial free energy of the resulting strands leads to bundling and the evolution of fibrillar structures. These aggregates intertwine and develop into a three-dimensional gelator network. Since this self-assembled fibrillar network (SAFiN) is based on intermolecular interactions, i.e. H-bond, London dispersion forces, their formation is thermoreversible. Depending on the gelator concentration the gel-sol transition occurs around 65–80 °C. The SAFiN-mesh structure depends on the cooling rate during the preparation process. The slower the cooling rates the longer the annealing time of the fibre growth resulting in a small number of permanent nodes originating from crystalline mismatch branching. If the high temperature sol is quenched to room temperature, the branching grade intensifies, a SAFiN containing high numbers of nodes evolves [54–65].

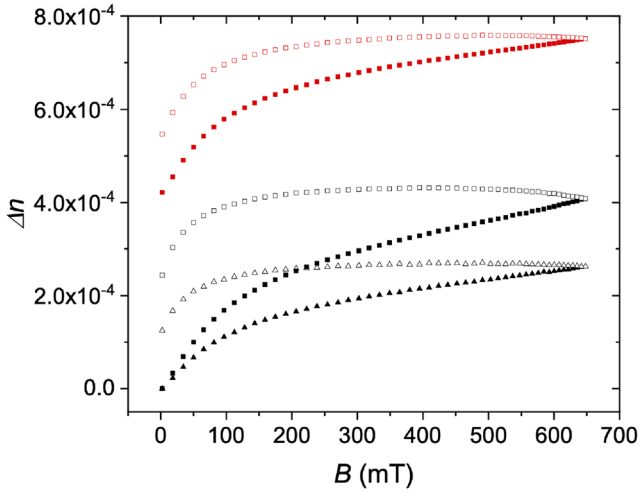

Figure 5: Magnetically induced birefringence $\Delta n(B)$ in an isotropic (black squares – 1st run, black triangles – 2nd run) and an anisotropic (red triangles) gel with 10 wt% MNP and 12.5 wt% gelator concentration at room temperature. Filled symbols correspond to increasing field and empty symbols to decreasing field. (Adopted from a study by Nádasi et al. [37]).

The gel structure was characterized by atomic force microscopy and scanning electron microscopy (SEM). A mosaic of spherulitic domains with a radial distribution of fibres can be seen in the low-magnification SEM images (Figure 6a), whose appearance is consistent with the textures observed by polarizing optical microscopy. High-magnification images (Figure 6b) reveal an interwoven structure of thin 32 ± 6 nm fibres in a gel with 10 wt% gelator. At this length-scale, the fibres appear disordered, forming a mesh with an average size of 60 ± 25 nm. This mesh size is significantly larger than the particle diameter (10 nm). Therefore, one mesh cell may accommodate short chains with 4–8 MNPs. The solvent-gelator compatibility of APG2135 with 12-HOA is comparable to that of a nonpolar solvent, since the ferrofluid can be considered as a nonpolar liquid with superparamagnetic properties. However, exactly the response of the sol in a magnetic field enables additional fine-tuning of the properties of the ferrogel.

To prepare the isotropic ferrogels, the sample was quenched to room temperature (cooling rate > 50 K min^{-1}). In the case of anisotropic ferrogels, the heated sample was cooled down at a controlled cooling rate (1 K min^{-1}) in a magnetic field of 650 mT. The samples were prepared in 100-μm thick rectangular capillaries. Bars of ferrogels easily bend upon bringing them in a magnetic field gradient. This demonstrates that despite the MNPs are dispersed in the liquid subphase, there is coupling between magnetic and elastic degrees of freedom.

This coupling is confirmed by our magneto-optical measurements. In Figure 5, the magnetic field dependence of the birefringence of an isotropic gel measured by optical

modulation technique is shown. The two distinctively characteristic features of those curves are the hysteresis originating from the difference between the birefringence measured in increasing and decreasing magnetic field and the lowering of the birefringence values in the second measurement.

In the first measurement, the isotropic gel is exposed to a magnetic field for the first time. As described above, the viscoelastic matrix hinders the perfect alignment of the embedded MPs along the magnetic field. The competition between the aligning magnetic dipoles and the viscoelastic deformation of the matrix leads to some irreversible deformations in favour of better alignment of the magnetic dipoles. In the meantime, this interaction facilitates the adsorption of the particles along the cavity walls, resulting in a fewer number of free MPs contributing to the chain formation in the second run. Therefore, the birefringence of the isotropic gel in the second run is lower. The hysteresis is the consequence of the viscoelastic deformations of the gel network. The relaxation of the network to the initial state is a long-term process. In fact, after a full measurement cycle (0 mT → 650 mT → 0 mT), it takes at least 10 h for the gel to relax in absence of the magnetic field to a constant birefringence close to the initial one. The hysteresis of the first run is always bigger than that of the second run corroborating the idea of the matrix inelastic deformations.

Anisotropic gels prepared by a slow cooling from the sol state exhibit a striped birefringent texture in polarizing microscopy, where the stripes are aligned along the field direction applied during the preparation.

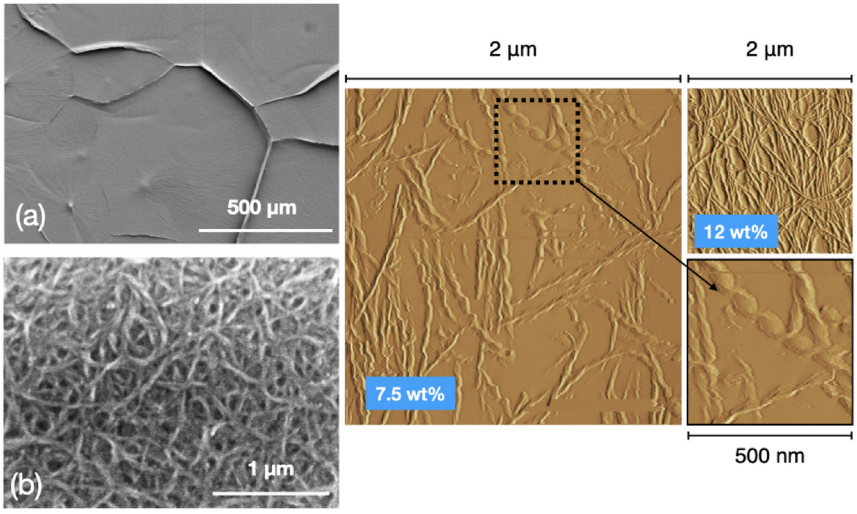

Figure 6: Scanning electron microscopy images of an isotropic gel with 7 wt% of the MNPs and 10 wt% of the gelator at (a) low magnification and (b) high magnification. (U = 1.5) kV. (c) Atomic force microscopy images of the gels with 7.5 wt% and 12.5 wt% of the gelator (4.5 wt% of MNPs). The inset shows a magnified image of a helical nanofilament. (Adopted from a study by Nádasi et al. [37]).

The high birefringence of the anisotropic gels in Figure 7d can be explained by the formation of MNP chains in the initial high temperature sol state. As in the ferrofluid, the higher the applied field the bigger is the birefringence of the sol, and no hysteresis can be observed (Figure 7c). Since the magnetic field is applied throughout the whole preparation process, the chains do not fall apart and they give rise to a direction dependent evolution of the gel network. Additionally, the gradual slow cooling increases the annealing time of the gel fibre growth resulting in less branching. Altogether, the mesh network is expected to be looser, especially in the direction of the applied preparation field. If no magnetic field is present, the MNP chains fall apart, yet the direction dependent growth of the fibres produces an optical anisotropy, i.e. birefringence. That is why the initial birefringence of the anisotropic gels is always higher than of the isotropic ones (Figure 7d). Since the MNP chain formation in the gel is facilitated in the external field direction, i.e. the optical axis is aligned to the magnetic field, the following phenomena are observed:

– the $\Delta n(B)$ curves coincide in repeated measurements,

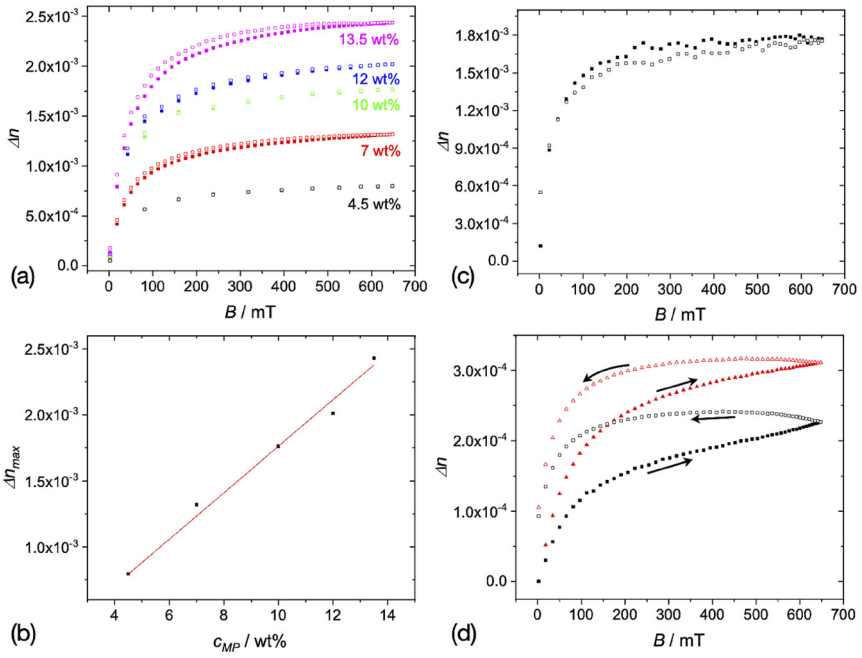

Figure 7: (a) Birefringence $\Delta n(B)$ of the ferrofluid APG2135 diluted with n-dodecane. (b) Saturation birefringence Δn_{max} as a function of the concentration of the MNPs c_{MP} in the ferrofluids. (c) Birefringence $\Delta n(B)$ of a dispersion of 13.5 wt% MNPs and 10 wt% 12-HOA at $T = 80\ ^{\circ}C$ (sol). No significant hysteresis behaviour can be found for a dwell time of 30 s. (d) Magnetically-induced birefringence $\Delta n(B)$ in an isotropic (black squares) and an anisotropic (red triangles) gel with 4.5 wt% MNP and 7.5 wt% gelator concentration at room temperature. Filled symbols correspond to increasing field and empty symbols to decreasing field. (Adopted from a study by Nádasi et al. [37]).

- the birefringence is higher in the anisotropic gel with the same c_G and c_{MP} for any applied field,
- the hysteresis of the anisotropic gels is always smaller than for the isotropic gels with the same c_G and c_{MP}.

The birefringence decreases, changing its sign if the measuring field is perpendicular to the anisotropy axis. Varying the concentration of the MNPs (c_{MP}) and the gelator (c_G) enables fine-tuning of the optical properties of the organoferrogel (Figures 8 and 9a, b).

An increasing gelator concentration provides negative feedback on the magneto-optical response: the saturating birefringence decreases with increasing gelator concentration (Figure 9c, d). However, the dependence $\Delta n(c_G)$ remains linear in the investigated concentration range (Figure 11b, d).

There is a clear difference between the isotropic and the anisotropic gels if one considers the slopes $s(c_G) = d\Delta n(c_{MP})/dc_{MP}$. The slope s for low concentration of the gelator is nearly independent on the concentration. This can be understood by assuming that at low gelator concentrations, the mesh is loose in the anisotropy direction. The gel mesh has less confinement effect on the growth of the magnetic aggregates. For higher gelator concentration (12.5 wt%), the gel network restricts the growth and the slope $s(c_G)$ becomes reduced. The hysteresis $h(c_{MP})$ increases with increasing MNP concentration c_{MP} in both isotropic and anisotropic gels. However, the isotropic gels have a systematically lower birefringence and larger magneto-optical hysteresis (Figure 10).

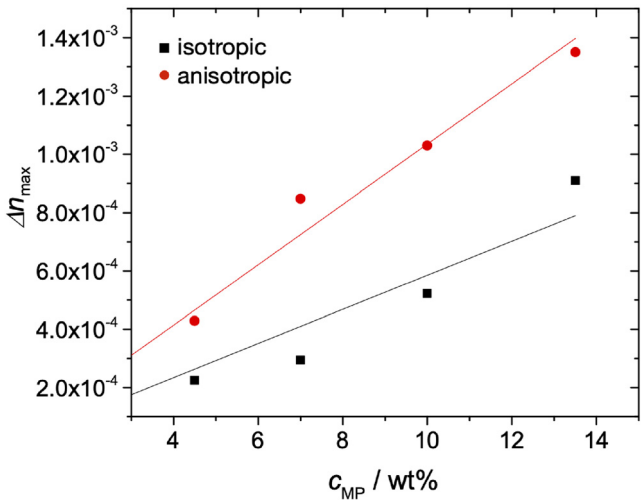

Figure 8: Magnetic particle concentration dependence of the saturation birefringence $\Delta n_{max}(c_{MP})$ for isotropic and anisotropic gels with 10 wt% gelator. The straight lines are linear fits under the constraint $\Delta n_{max}(0) = 0$. (Adopted from a study by Nádasi et al. [37]).

Figure 7d shows the field dependence of the birefringence $\Delta n(B)$ for a gel with a gelator concentration of 10 wt%. The field dependence of the birefringence $\Delta n_{+}(B)$ and $\Delta n_{-}(B)$ on increasing and decreasing magnetic field B, respectively, differ considerably. Only $\Delta n_{-}(B)$ can be satisfactory fitted with the Eq. (8) in gels with the gelator concentration below 10 wt%. To estimate the hysteresis strength, we introduce a dimensionless parameter h:

$$h = \frac{\int_0^{B_{\max}} \Delta n_{-}(B)\mathrm{dB} - \int_0^{B_{\max}} \Delta n_{+}(B)\mathrm{dB}}{\int_0^{B_{\max}} \Delta n_{-}(B)\mathrm{dB}} \tag{6}$$

where $B_{\max} \to \infty$. In our experiment, $B_{\max}$ was limited to 650 mT.

It is important to mention that these gels show no magnetic hysteresis. The magnetic relaxation in our system is governed by the Néel relaxation mechanism with corresponding relaxation rates in the range of 100 MHz. Thus, the magnetization rapidly adjusts to the applied magnetic field on a very short (compared to our experiment) time scale. The birefringence response Δn has two important contributions: the birefringence Δn_{MP} attributed to the aligned magnetic chains and the birefringence Δn_{G}

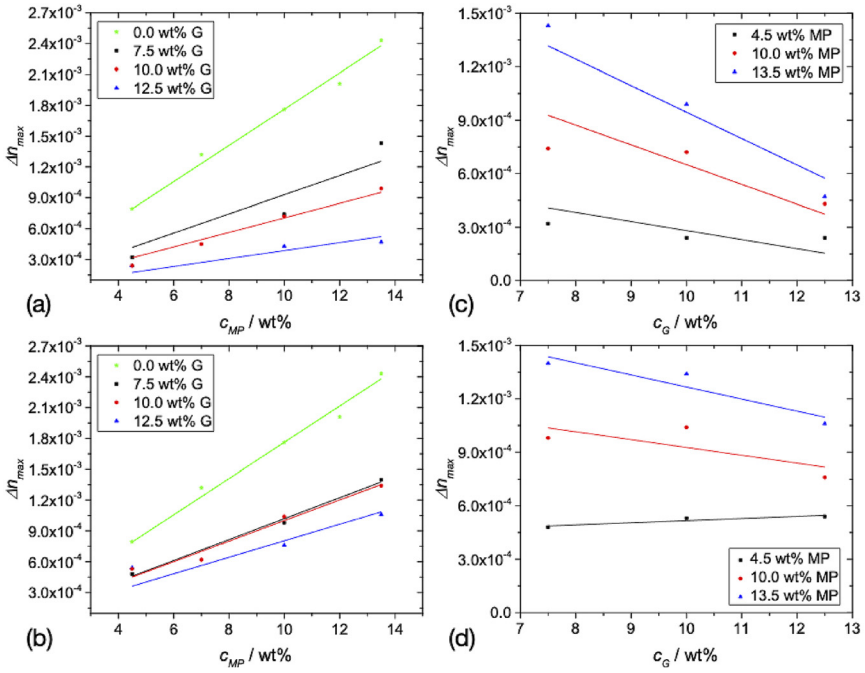

Figure 9: Dependence of the saturation birefringence $\Delta n_{\max}$ of the ferrogel on the concentration of the MPs c_{MP} in the isotropic (a) and the anisotropic (b) gels. Dependence of the saturation birefringence $\Delta n_{\max}$ of the ferrogel on the concentration of the gelator c_{G} in the isotropic (c) and the anisotropic (d) gels. (Adopted from a study by Nádasi et al. [37]).

caused by a deformation of the gel matrix. In a dilute limit, the relaxation times for Δn_{MP} can be estimated as the time an MNP requires to diffuse over a distance of particle radius R, $\tau = 6\pi\eta R^3/kT$, where η is the viscosity of the matrix, T is the temperature. For dodecane, $\tau \approx 0.2$ µs. In the gel state, the situation is much more complex. The viscosity increases by several orders of magnitude and the environment of the particles becomes strongly heterogeneous. Particles interact with the gel network. Already at $c_G = 3$ wt%, τ reaches the order of magnitude of a second. A slow increase of the birefringence in a magnetic field can also be attributed to slow deformations of the gel network and the adhesion of MNPs to the gel fibres. This also results in a residual birefringence which relaxes on the time scale of days. The dynamical properties of the mobile NPs in the gel matrix will be discussed in an upcoming paper.

The behaviour of the saturating birefringence Δn_{max} and the hysteresis parameter h show the effect of the local anisotropy of the gel, which is a surprising finding because the sizes of the particles are smaller than the mesh size of the gel. Larger Δn_{max} and smaller h suggests that MNPs have more space to rearrange and form larger aggregates along the anisotropy axis. Birefringence in MNP agglomerates results from the mutual polarizability of adjacent MNPs [42, 66]. The association of MNPs into chains was described in the early seventies by P.G. de Gennes and P.C. Jordan using hard-sphere models [40, 41, 67]. The formation of MNP dimers reduces the entropy of the system and shifts the equilibrium from single particles to dimers [67, 68].

The effective dielectric tensor $\hat{\varepsilon}_{eff}$ of the composite fluid can be decomposed into the isotropic part $\hat{\varepsilon}_{host}$ of the host fluid and the anisotropic part of the inclusions $\hat{\varepsilon}_{inc}$:

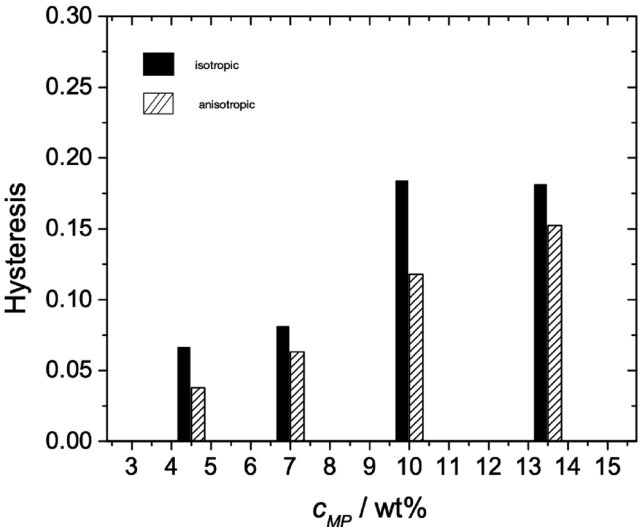

Figure 10: Dependence of the hysteresis parameter h on the concentration of the magnetic particles c_{MP}. (Adopted from a study by Nádasi et al. [37]).

$\hat{\varepsilon}_{\text{eff}} = \hat{\varepsilon}_{\text{host}} + \hat{\varepsilon}_{\text{inc}}$. The dielectric polarizability α of the anisometric MNP aggregates is anisotropic. In case of magnetic chains, the length of the chain and the intrinsic optical properties of MNPs determine the polarizability anisotropy $\Delta\alpha$. In the thermal equilibrium, the alignment of the chains is subject to thermal fluctuations. The components of the dielectric permittivity of the chains are given by the average

$$\varepsilon_{\text{inc}_j} = \frac{1}{\varepsilon_0} \sum_{k=1}^{\infty} \varphi(k) \langle \alpha_j \rangle_{\theta,\phi} \tag{7}$$

where the summation runs over all chains of the length k with the volume fraction $\varphi(k)$, respectively. The averaging is done over all possible orientations θ, ϕ.

The field-dependence of the birefringence induced by the dimerization in a magnetic fluid was studied by several authors [42, 44, 66, 69–72]. Assuming a Boltzmann orientational distribution of the particle pairs, the birefringence attributed to the dimers can be found from Janssen's dependence [66, 72]:

$$\Delta n(x) = \varphi_2 A \left(1 - 3\left(\frac{\coth(x)}{x} - \frac{1}{x^2}\right)\right) \tag{8}$$

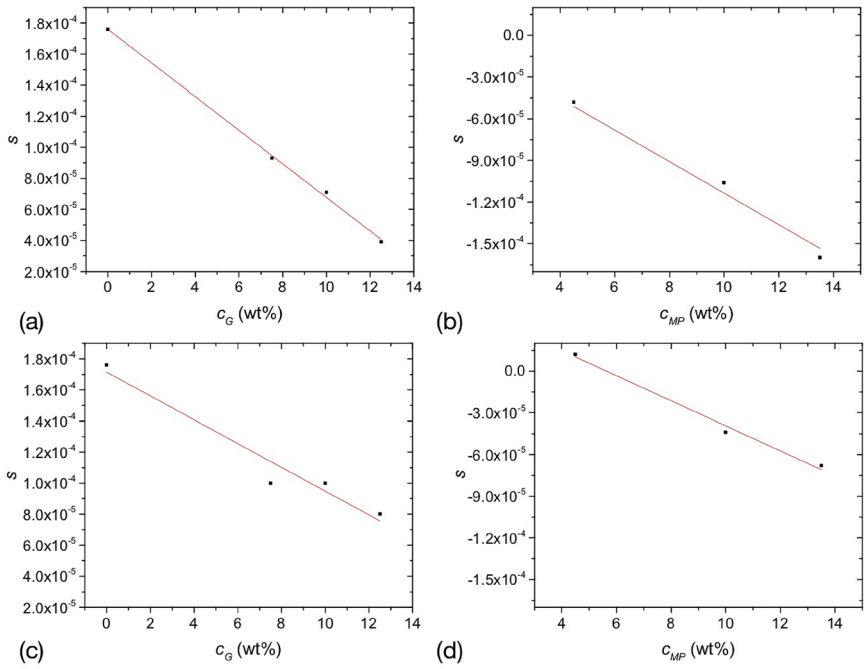

Figure 11: (a) and (c) show the slopes s of linear fits of $\Delta n_{\max}(c_{\text{MP}})$ as functions of the gelator concentration in the isotropic and anisotropic gels, respectively. Figures (b) and (d) show the slopes s of the linear fits of $\Delta n_{\max}(c_{\text{G}})$ as functions of the MNP concentration of the isotropic and anisotropic gels, respectively (Adopted from a study by Nádasi et al. [37])

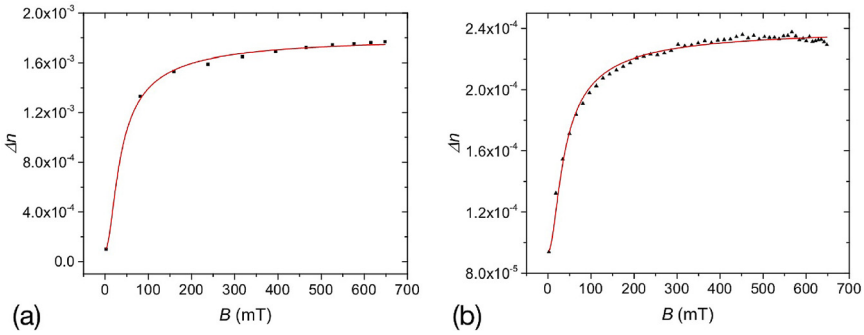

Figure 12: Magnetically induced birefringence $\Delta n(B)$ as a function of the field strength B in (a) ferrofluid with $c_{MP} = 10.4$ wt% and (b) ferrogel with $c_{MP} = 4.5$ wt% of MNPs and $c_G = 12.5$ wt%. The solid red lines are fits using Eq. (8).

where $x = \mu_{aggr}B/kT$b, and μ_{aggr} is the magnetic moment of the chain aggregate, T is the temperature and k_b is the Boltzmann constant. The factor A is determined by the polarizabilities of the particles.

Equation (8) describes well the experimental observations in pure ferrofluids and in the sol state (Figure 12). From the fit of $\Delta n(B)$, we deduce the magnetic moment of the chain-aggregate $\mu_{aggr} = 4.28{\cdot}10^{-19}\text{Am}^2$. This corresponds roughly to two MNPs. The volume fraction of magnetic dimers is determined by the magnetic field and the temperature. In the gel state, however, this description fails. Satisfactory fits can be found mostly for Δn with decreasing field B for low concentrations of MNP and the gelator. The reason for that is the nonequilibrium behaviour of $\Delta n(B)$. The deformation of the gel network occurs on much slower time scales than the rearrangement of the MNPs.

5 Magnetic suspensions in rotating fields

5.1 Rotational effect

Among the phenomena that attracted particular attention of researchers of magnetic liquids, the magnetic torque transfer in rotating or oscillating magnetic fields remains incompletely understood. Macroscopic samples of magnetic fluids have a tendency to develop vortex flow when exposed to rotating magnetic fields. For this phenomenon, the term rotational effect [73–79] has been coined. It turns out that this effect depends on sample geometries, free surfaces of the fluid, the composition (polydispersity) of the magnetic fluid, as well as frequencies and magnitudes of the magnetic field in a complex way. This effect can not only be used to transfer torque to the container or immersed objects [78], it can be exploited to study negative viscosity effects [80, 81], to rectify thermal motion [82, 83] or to characterize structural sample properties [84, 85].

Numerous studies in literature were devoted to magnetic fluids exposed to external rotating or oscillating magnetic fields, see, e.g. references in a study by Storozhenko et al. [84]. We focus here on two detailed aspects of this effect, on the study of diluted ferrofluids in order to reveal the role of viscosity on the efficiency of the torque transfer [84] and an analysis of the frequency and field strength dependence on the composition and microscopic parameters of the magnetic fluid.

5.2 Torsion pendulum setup

When a magnetic fluid is exposed to a magnetic field that exerts a permanent torque on the MNPs, this torque is transferred to the carrier fluid to create a vortex flow, and further to the container by shear forces of the flowing liquid at the container walls. If the container is freely suspended, the rotation is continuously accelerated [82], the measurement of the torque from the angular velocity profile of the container is difficult. Therefore, a torsion pendulum is a reasonable alternative, it measures the distortion of the suspending wire in equilibrium of the magnetic field–induced torque with the restoring elastic torque of the wire. Figure 13 sketches the setup [83, 84].

The magnetic field is generated by two sinusoidal currents, with 90° phase shift, in two pairs of coaxial coils, and monitored with Hall probes. The samples are enclosed by spherical glass containers of approximately 1 mL volume. The sensitivity of the setup

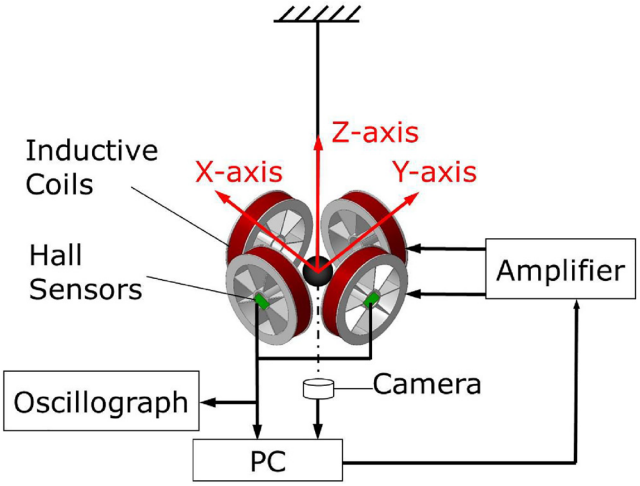

Figure 13: Torque balance setup for the measurement of the rotational effect in ferrofluids. The magnetic field is generated with two pairs of coaxial coils [83, 84]. The torque is measured from the twist of the suspending thread. The sample container is partly immersed in an oil bath to dampen the pendulum oscillations in order to reach the equilibrium deflection faster, and to attenuate influences of external noise. Figure adapted from a study by Storozhenko [84].

allows us to measure torque densities of the order of 10^{-4} N/m^2 (torques of 10^{-10} Nm on the samples), angular frequencies were typically of the order of 50 s^{-1} to 5000 s^{-1}, in some experiments up to 30,000 s^{-1}, field strengths up to a few mT were applied. The sample was suspended by a thin glass fibre, with very low restoring torque, so that the eigenfrequency of the pendulum was below 100 mHz.

5.3 Diluted ferrofluids and viscosity effects

The transfer of the magnetic torque onto the suspending fluid occurs in two steps: in the first step, the external magnetic field interacts with the magnetization of the MNPs. In a second step, this torque is transferred to the carrier fluid by viscous forces. The torque excerted by a field $\vec{B}$ on the magnetic moment $\vec{m}$ of an individual NP is $\vec{T} = \vec{m} \times \vec{B}$. This torque is proportional to sinα, with α being the angle between $\vec{m}$ and $\vec{B}$. In the at moderate rotation rates $\omega = \dot{\varphi}$ of $\vec{B} = B(\cos\varphi, \sin\varphi, 0)$, the magnetization follows the field after a short transient with the same angular velocity but a constant phase lag α. Two different mechanisms compete in the reorientation of $\vec{m}$. The particles themselves may rotate, with $\vec{m}$ being fixed relative to the MNP. This process is usually referred to as Brownian relaxation. It depends upon the viscosity of the carrier fluid that dampens the rotation of particles relative to the matrix. The higher this viscosity, the larger is the phase lag α and the larger is the magnetic torque at given B, $\left|\vec{m}\right|$, and ω. The second process is the reorientation of the magnetization $\vec{m}$ relative to the particle orientation, referred to as Néel relaxation. When the particles are small, this is the prevailing mechanism. Here, α does not depend upon the rotation state of the MNP, and is thus

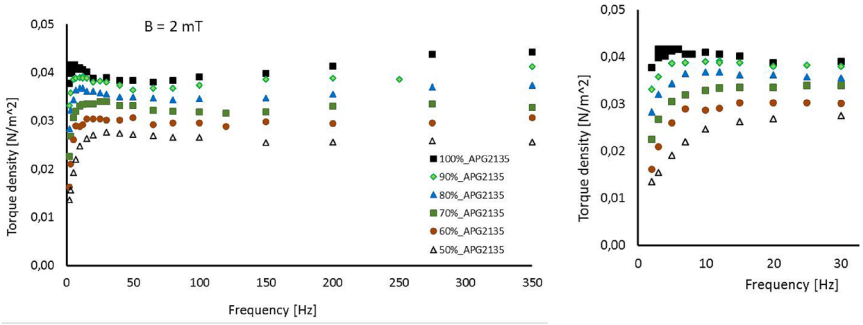

Figure 14: Torque density in samples with different concentrations of the original ferrofluid. The right graph is an expansion of the low-frequency region of the graph at the left. Figure adapted from a study by Storozhenko et al. [84].

independent of viscosity, even though the transfer of the magnetic torque from the MNPs to the carrier fluid still proceeds by viscous shear forces.

In order to explore the influence of viscosity of the magnetic fluid on the torque transfer, a commercial ferrofluid (APG2135, *Ferrotec Corp. (Japan)*) with a viscosity of 1.5 Pas was diluted with different concentrations of durasyn (viscosity 46 mPas). If the internal structure of the magnetic fluid were independent of the applied magnetic field, the torque would be proportional to the MP concentrations, and it would continuously increase with increasing rotation rate of the magnetic field. This is the consequence of an increasing phase lag between the sample magnetization and $\vec{B}$ with increasing ω. This condition is in fact fulfilled only for well-diluted samples. Experimental results are seen in Figure 14.

The decrease of the torque density is smaller than expected from the decrease of MNP concentration in the range of up to 50 % dilution. On the other hand, the change of viscosity by roughly one order of magnitude apparently has only little effect on the graphs. A certain saturation of the torque density is found at comparable rotation rates. If the torque was primarily generated from Brownian relaxation, one would expect that it would substantially decrease in the diluted samples.

A characteristic difference between the high-concentration and diluted systems is a slight elevation of the torque characteristics at rotation frequencies below 10 Hz. This was attributed to the formation of small particle aggregates at higher fields, which would increase the magnetic response. At larger rotation rates, these agglomerates decompose since they cannot follow the field direction. Then, the torque drops in the range between 10 and 50 Hz for the highly concentrated suspensions.

The torque transfer is also influenced by the rheological properties of the carrier fluid. This was demonstrated by addition of nonmagnetic platelet-shaped pigment particles [86]. When the isotropic solvent (n-dodecane) is replaced by anisometric crystallites, the character of the torque characteristics changes substantially owing to the non-Newtonian character of the concentrated pigment particle suspensions

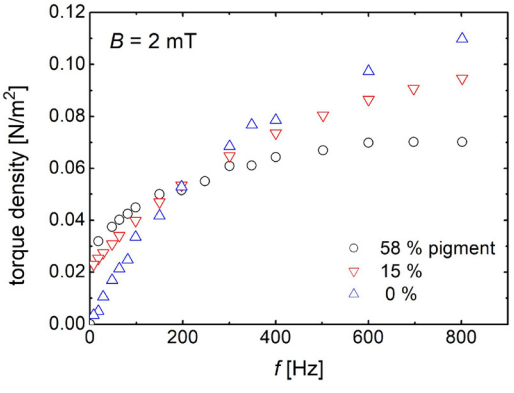

Figure 15: Torques on ternary mixtures of ferrofluid, dodecane and Permanent Rubine pigment particles. The ferrofluid concentration is 40%, the concentrations of pigment particles are given in the legend, the rest is dodecane. Printed with kind permission of A. Storoshenko [84].

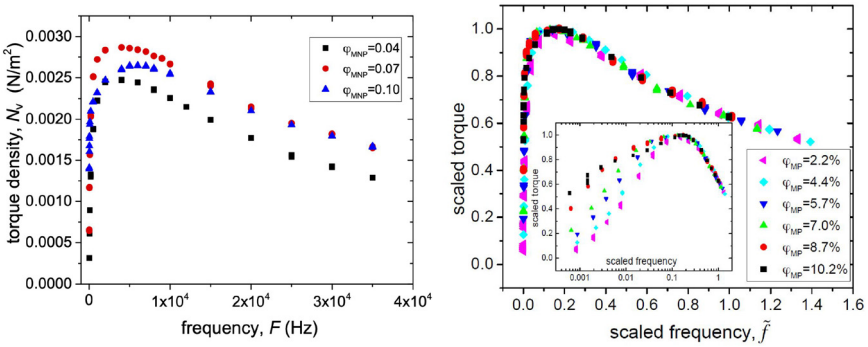

Figure 16: Left: Frequency dependence of the magnetic torque density in dispersions with various volume fractions φ_{MNP} of magnetic particles. Right: Scaled torque dependencies N_v/N_{max} ($\tilde{f}$) for dispersions with different volume fractions of magnetic particles. Note the extended frequency range as compared to Figure 14. Reprinted from a study by Usadel et al. [85].

Figure 15. The saturation of the torque shifts to lower frequencies. This reflects the interactions of the flow generated by the MNPs and the anisometric platelets.

5.4 Néel and Brownian relaxation in rotating fields

So far, we have disregarded the nature of the interactions between the MNP magnetizations and the external field. A closer analysis shows that in fact, the Néel relaxation time τ is dominant for most of the magnetic NPs contained in commercial ferrofluids. The quantitative analysis shows that the crossover from predominant Néel relaxation of small MNPs to Brownian relaxation of large MNPs in polydisperse samples occurs near 10 nm particle diameter. Smaller MNPs represent by far the majority of particles in typical ferrofluids, so that most of the particles are characterized by an internal relaxation of the magnetization. On the other hand, the magnetization of individual particles grows with the third power of their diameter, so that relatively few large particles still contribute noticeably to the magnetic torque. These processes were analysed recently in a combined theoretical and experimental study [85]. Magnetic torques were measured with the torque balance technique over an extended frequency range up to 35 kHz.

The original ferrofluid synthesized in the Scientific Research Laboratory of Applied Ferrohydrodynamics (ISPU, Ivanovo) by chemical condensation consists of single-domain spherical nanoparticles of magnetite Fe_3O_4 stabilized by oleic acid and dispersed in kerosene. It was stepwise diluted with dodecane (viscosity: 1.34 mPas) so that the concentration of MNPs ranged from 10.2 to 2.2%, while the viscosity dropped with increasing dilution from about 30 mPas down to 2 mPas. Figure 16 shows the experimental findings. At higher frequencies (beyond the torque maximum) all graphs can be scaled to a master curve. At low frequencies, there are some systematic

deviations that most probably stem from aggregation of single MNPs in the higher concentration range.

Measurements of the magnetic torque of diluted dispersions of MNPs in rotating magnetic fields and the comparison to numerical simulations have demonstrated the crucial importance of the distribution of particle sizes. From a theoretical point of view, it was shown that the rigid dipole model (RDM), which fixes the magnetization in the particle, cannot explain the experimental observations. It predicts that the torque and other dynamical features depend only on the product of the viscosity and rotation rate of the external field. In order to understand the experimental results, it is necessary to take both Brownian and Néel relaxation into account [85]. The theoretical results show that in a rotating magnetic field a transition takes place from a state with the magnetic moment locked to the anisotropy axis of the MNPs to a state with precessional spin dynamics. This transition depends on the anisotropy energy. The dependence of the anisotropy energy on the magnetic volume of the MNPs causes an essential dependence on particle sizes. This must be taken into account in all experiments performed with diluted ferrofluids of a broad distribution of particle sizes.

For MNPs at room temperature with magnetic parameters typical for iron oxides (such as magnetite), the magnetic moment can be considered as being locked if the magnetic radius is larger than about 10^{-8} m [85]. Such particles can be described analytically within the RDM. For smaller particles, both Brownian and Néel dynamics are relevant, and a numerical analysis is required. The faster Néel relaxation decreases the relaxation time, and consequently the phase lag of the magnetization and the transferred torque considerably.

These conclusions apply to most of the commercial ferrofluids widely used in applications, which are commonly characterized by broad distributions of particle sizes. The theoretical analysis shows that much larger torques could be achieved with particles with larger anisotropy constant. Such particles would be similarly stable, e. g. with respect to aggregation, but the critical radius above which Brownian relaxation dominates would become much smaller, so that more particles contribute to a large torque. An experimental confirmation of this theoretical prediction is a desirable goal of future research.

6 Summary

Experimental and MD simulation of cosuspensions of non-magnetic anisotropic microcrystallites and magnetic nanoparticles have demonstrated an efficient orientation transfer from the magnetic subphase to the non-magnetic one, even with shape-isotropic MNPs. In relatively low magnetic fields (up to 700 mT), suspensions of the non-magnetic pigment particles alone show very low magnetically induced birefringence. The magneto-optical response is drastically enhanced by addition of a small

volume fraction of MNPs. The form anisotropy of the non-MPs plays a crucial role in this effect. The gain of translational entropy resulting from the alignment of the elongated non-MPs with anisometric aggregates of the MNP dopants drives the reorientation of the nonmagnetic subphase. This alignment is particularly well pronounced in platelet-shaped nanocrystallites of Pigment Red 176, which shows an exceptionally large magneto-optical response [87].

Addition of MNPs to thermotropic liquid-crystalline phases also generates magneto-optical effects or alters the magneto-optical response of the doped LCs [27]. However, the measured effects are substantially weaker than with the magnetically doped suspensions. The stability of the samples is a substantial problem, the nematic host prefers to expel the dopants or to collect it in defect structures. The interactions of the MNPs with the LC matrix depend crucially on the MNP surface chemistry. The doped LC materials did not show any qualitatively new features, but quantitative effects are observed, and they can be explained satisfactorily.

In fibrillous gels, the motion of included MNPs is restricted by the gelator network with a mesh size comparable to the MNPs. We investigated the structure and the magneto-optical response of isotropic and anisotropic fibrillous organoferrogels with mobile MNPs. The presence of the gel network restricts the magneto-optical response of the ferrogel. Even though the ferrogel exhibits no magnetic hysteresis, an optical hysteresis has been found. This suggests that the optical response is primarily determined by the dynamics of self-assembly of the embedded MNPs into shape-anisotropic agglomerates. The optical anisotropy of the system can be fine-tuned by varying the concentrations of the gelator and the MNPs. The optical response in structurally anisotropic gels is orientation-dependent, revealing an intricate interplay between the confining mesh and the MNPs [37].

The torque measurement technique introduced in Section 5 can determine magnetic torques with nanonewton accuracy. It was demonstrated to provide useful results both for ferrofluids and for suspensions of nonmagnetic pigment crystallites and magnetic nanoparticles. Torques generated in conventional ferrofluids composed of spherical particles are quite small because Néel relaxation that dominates the dynamics of small nanoparticles is much faster than usual rotation rates of the magnetic field. The transferred torque depends upon the phase lag of the sample magnetization respective to the rotating external magnetic field, which is extremely small in typical spherical MNPs [85]. A strategy to achieve substantially larger torques would be the use of shape-anisotropic MNPs, in which the magnetization is pinned to the particle and the relaxation is governed by Brownian motion of the MNPs. The phase lag is substantially larger in that case even at slow rotation rates. Potential applications of this method are manifold, including the study of rectified thermal motions of MNPs in an oscillating field, using a ratchet effect [83, 84].

Acknowledgment: The German Science Foundation is acknowledged for funding within projects STA 425/36-(1-3) in the priority program SPP1681, and the Council for grants of the President of the Russian Federation is acknowledged for Grant No. 075-15-2019-743. The authors acknowledge important contributions by K. Usadel to theoretical modeling, and A. Storoshenko and Á. Corradi to the experiments. Valuable collaborations with the groups of A. Schmidt, S. Klapp, and S. Behrens within SPP 1681 are gratefully acknowledged.
Author contribution: All the authors have accepted responsibility for the entire content of this submitted manuscript and approved submission.
Research funding: German Science Foundation STA 425/36-(1-3) in the priority program SPP1681, Council for Grants of the President of the Russian Federation Grant No. 075-15-2019-743.
Conflict of interest statement: The authors declare no conflicts of interest regarding this article.

References

1. Onsager L. Anisotropic solutions of colloids. Phys Rev 1942;62:558.
2. Onsager L. The effects of shape on the interaction of colloidal particles. Ann N Y Acad Sci 1949;51: 627–59.
3. Vroege GJ, Lekkerkerker HNW. Phase transitions in lyotropic colloidal and polymer liquid crystals. Rep Prog Phys 1992;55:1241–309.
4. Davidson P, Gabriel J-CP. Mineral liquid crystals. Curr Opin Colloid Interf 2005;9:7–7.
5. Gompper G, Schick M. Soft matter: volume 3: colloidal order: entropic and surface forces. Germany: Wiley-VCH; 2007.
6. Grelet E, Lettinga MP, Bier M, van Roij R, van der Schoot P. Dynamical and structural insights into the smectic phase of rod-like particles. J Phys Condens Matter 2008;20:494213.
7. van der Beek D, Petukhov AV, Oversteegen SM, Vroege GJ, Lekkerkerker HNW. Evidence of the hexagonal columnar liquid-crystal phase of hard colloidal platelets by high-resolution SAXS. Eur Phys J E 2005;16:253–8.
8. van der Beek D, Reich H, van der Schoot P, Dijkstra M, Schilling T, Vink R, et al. Isotropic-nematic interface and wetting in suspensions of colloidal platelets. Phys Rev Lett 2006;97:087801.
9. van der Beek D, Petukhov AV, Davidson P, Ferré J, Jamet JP, Wensink HH, et al. Magnetic-field-induced orientational order in the isotropic phase of hard colloidal platelets. Phys Rev E 2006;73: 041402.
10. Lemaire BJ, Davidson P, Ferré J, Jamet J-P, Petermann D, Panine P, et al. The complex phase behaviour of suspensions of goethite (alpha-FeOOH) nanorods in a magnetic field. Faraday Discuss 2005;128:271–83.
11. Lemaire BJ, Davidson P, Ferré J, Jamet JP, Panine P, Dozov I, et al. Outstanding magnetic properties of nematic suspensions of goethite (alpha-FeOOH) nanorods. Phys Rev Lett 2002;88:125507.
12. Meuer S, Oberle P, Theato P, Tremel W, Zentel R. Liquid crystalline phases from polymer-functionalized TiO2 nanorods. Adv Mater 2007;19:2073.
13. Fraden S, Hurd AJ, Meyer RB, Cahoon M, Caspar DLD. Magnetic-field-induced alignment and instabilities in ordered collloids of tobacco mosaic virus. J Phys Colloq 1985;46:85–113.

14. Dogic Z, Fraden S. Smectic phase in a colloidal suspension of semiflexible virus particles. Phys Rev Lett 1997;78:2417–20.
15. Dogic Z, Fraden S. Cholesteric phase in virus suspensions. Langmuir 2000;16:7820–4.
16. Purdy KR, Dogic Z, Fraden S, Rühm A, Lurio L, Mochrie SGJ. Measuring the nematic order of suspensions of colloidal fd virus by X-ray diffraction and optical birefringence. Phys Rev E 2003;67: 627.
17. Fraden S, Hurd A, Meyer RB. Electric-field-induced association of colloidal particles. Phys Rev Lett 1989;63:2373–6.
18. Kredentser S, Buluy O, Davidson P, Dozov I, Malynych S, Reshetnyak V, et al. Strong orientational coupling in two-component suspensions of rod-like nanoparticles. Soft Matter 2013;9:5061.
19. Lekkerkerker HNW, Coulonvan der Haegen PR, Deblieck R. On the isotropic-liquid crystal phase separation in a solution of rodlike particles of different lengths. J Chem Phys 1984; 80:3427.
20. Schmidt MU, Hofmann DW, Buchsbaum MC, Metz HJ. Crystal structures of pigment red 170 and derivatives, as determined by X-ray powder diffraction. Angew Chem Int Ed 2006;45:1313–17.
21. May K, Eremin A, Stannarius R, Peroukidis SD, Klapp SH, Klein S. Colloidal suspensions of rodlike nanocrystals and magnetic spheres under an external magnetic stimulus: experiment and molecular dynamics simulation. Langmuir 2016;32:5085–93.
22. Eremin A, Geng Y, Stannarius R, Ostapenko T, Challa PK, Gleeson JT, et al. Peculiarities of the magneto-optical response in dispersions of anisometric pigment nano-particles. RSC Adv 2016;6: 80666–9.
23. Herzfeld J, Berger AE. A highly convergent algorithm for computing the orientation distribution functions of rodlike particles. Macromolecules 1984;17:1718–23.
24. Slyusarenko K, Reshetnyak V, Reznikov Y. Magnetic field control of the ordering of two-component suspension of hard rods. Philos Trans A Math Phys Eng Sci 2013;371:20120250–20120250.
25. Peroukidis SD, Lichtner K, Klapp SHL. Tunable structures of mixtures of magnetic particles in liquid-crystalline matrices. Soft Matter 2015;11:5999–6008.
26. Peroukidis SD, Klapp SHL. Spontaneous ordering of magnetic particles in liquid crystals: from chains to biaxial lamellae. Phys Rev E 2015;92:010501.
27. Appel I, Nádasi H, Reitz C, Sebastián N, Hahn H, Eremin A, et al. Doping of nematic cyanobiphenyl liquid crystals with mesogen-hybridized magnetic nanoparticles. Phys Chem Chem Phys 2017; 504:1–9.
28. Zrínyi M, Barsi L, Büki A. Ferrogel: a new magneto-controlled elastic medium. Polym Gels Netw 1997;5:415–27.
29. Gollwitzer C, Turanov A, Krekhova M, Lattermann G, Rehberg I, Richter R. Measuring the deformation of a ferrogel sphere in a homogeneous magnetic field. J Chem Phys 2008;128:164709.
30. Varga Z, Filipcsei G, Zrínyi M. Smart composites with controlled anisotropy. Polymer 2005;46: 7779–87.
31. Jestin J, Cousin F, Dubois I, Ménager C, Schweins R, Oberdisse J, et al. Anisotropic reinforcement of nanocomposites tuned by magnetic orientation of the filler network. Adv Mater 2008;20:2533–40.
32. Krekhova M, Lattermann G. Thermoreversible organoferrogels: morphological, thermal and magnetic characterisation. J Mater Chem 2008;18:2842–8.
33. Krekhova M, Lattermann G, Schmalz H, Lang T, Richter R. Towards softer thermo-reversible magnetogels. Phys Procedia 2010;9:224–8.
34. Gollwitzer C, Krekhova M, Lattermann G, Rehberg I, Richter R. Surface instabilities and magnetic soft matter. Soft Matter 2009;5:2093–8.
35. Galicia JA, Cousin F, Dubois E, Sandre O, Cabuil V, Perzynski R. Static and dynamic structural probing of swollen polyacrylamide ferrogels. Soft Matter 2009;5:1–11.

36. Hasmonay E, Bee A, Bacri JC, Perzynski R. pH effect on an ionic ferrofluid: evidence of a thixotropic magnetic phase. J Phys Chem B 1999;103:6421–8.
37. Nadasi H, Corradi Á, Stannarius R, Koch K, Schmidt AM, Aya S, et al. The role of structural anisotropy in the magnetooptical response of an organoferrogel with mobile magnetic nanoparticles. Soft Matter 2019;15:3788–95.
38. Embs J, Müller HW, Krill CE, Meyer F, Natter H, Müller B, et al. Characterization of the grain size in ferromagnetic colloids: comparing torsional-pendulum measurements with standard complementary methods. Z Phys Chem 2006:153–71.
39. Embs JP, Huke B, Leschhorn A, Lücke M. Equilibrium and nonequilibrium behaviour of ferrofluids – experiments and theory. Z Phys Chem 2008;222:527–86.
40. de Gennes PG, Pincus PA. Pair correlations in a ferromagnetic colloid. Phys kondens Materie 1970; 11:189–98.
41. Jordan PC. Association phenomena in a ferromagnetic colloid. Mol Phys 1973;25:961–73.
42. Xu M, Ridler PJ. Linear dichroism and birefringence effects in magnetic fluids. J Appl Phys 1997;82: 326.
43. Ivanov AO, Kantorovich SS, Mendelev VS, Pyanzina ES. Ferrofluid aggregation in chains under the influence of a magnetic field. J Magn Magn Mater 2006;300:e206–9.
44. Ivanov AO, Kantorovich SS. Chain aggregate structure and magnetic birefringence in polydisperse ferrofluids. Phys Rev E 2004;70:021401.
45. Kantorovich SS. Chain aggregate structure in polydisperse ferrofluids: different applications. J Magn Magn Mater 2005;289:203–6.
46. Butter K, Bomans PH, Frederik PM, Vroege GJ, Philipse AP. Direct observation of dipolar chains in ferrofluids in zero field using cryogenic electron microscopy. J Phys Condens Matter 2003;15: S1451–70.
47. Odenbach S. Ferrofluids – magnetically controlled suspensions. Colloid Surface Physicochem Eng Aspect 2003;217:171–8.
48. Zubarev AY, Iskakova LY. Theory of structural transformations in ferrofluids: chains and "gas-liquid" phase transitions. Phys Rev E 2002;65:061406.
49. Sánchez PA, Gundermann T, Dobroserdova A, Kantorovich S, Odenbach S. Importance of matrix inelastic deformations in the initial response of magnetic elastomers. Soft Matter 2018;14:1–14.
50. Escuder B, Miravet JF, editors. Functional molecular gels. Soft Matter Series. Cambridge: Royal Society of Chemistry; 2013.
51. Guenet J-M. Organogels thermodynamics, structure, solvent role, and properties. Switzerland: Springer; 2016.
52. Terech P, Weiss RG. Low molecular mass gelators of organic liquids and the properties of their gels. Chem Rev 1997;97:3133–60.
53. van Esch JH, Feringa BL. New functional materials based on self-assembling organogels: from serendipity towards design. Angew Chem Int Ed 2000;39:2263–6.
54. Tachibana T, Mori T, Hori K. New type of twisted mesophase in jellies and solid films of chiral 12-hydroxyoctadecanoic acid. Nature 1979;278:578–9.
55. Co ED, Marangoni AG. Organogels: an alternative edible oil-structuring method. J Am Oil Chem Soc 2012;89:749–80.
56. Rogers MA, Wright AJ, Marangoni AG. Engineering the oil binding capacity and crystallinity of self-assembled fibrillar networks of 12-hydroxystearic acid in edible oils. Soft Matter 2008;4:1483–9.
57. Gao J. Solvent induced modifications to fiber nanostructure and morphology for 12HSA molecular gels [PhD thesis]. New Jersey: The State University of Rutgers; 2014.
58. Sakurai T, Masuda Y, Sato H, Yamagishi A, Kawaji H, et al. A comparative study on chiral and racemic 12-hydroxyoctadecanoic acids in the solutions and aggregation states: does the racemic form really form a gel?. Bull Chem Soc Jpn 2010;83:145–50.

59. Lan Y, Rogers MA. 12-Hydroxystearic acid SAFiNs in aliphatic diols – a molecular oddity. CrystEngComm 2015;17:8031–8.
60. Rogers MA, Marangoni AG. Kinetics of 12-hydroxyoctadecanoic acid SAFiN crystallization rationalized using hansen solubility parameters. Langmuir 2016;32:12833–41.
61. Terech P. 12-D-Hydroxyoctadecanoic acid organogels : a small angle neutron scattering study. J Phys II 1992;2:2181–95.
62. Lam R, Quaroni L, Pedersen T, Rogers MA. A molecular insight into the nature of crystallographic mismatches in self-assembled fibrillar networks under non-isothermal crystallization conditions. Soft Matter 2010;6:404–8.
63. Grahame DAS, Olauson C, Lam RS, Pedersen HT, Borondics F, Abraham S, et al. Influence of chirality on the modes of self-assembly of 12-hydroxystearic acid in molecular gels of mineral oil. Soft Matter 2011;7:7359–65.
64. Sato H, Hori K, Sakurai T, Yamagishi A. Long distance chiral transfer in a gel: experimental and ab initio analyses of vibrational circular dichroism spectra of R- and S-12-hydroxyoctadecanoic acid gels. Chem Phys Lett 2008;467:140–3.
65. Laupheimer M, Preisig N, Stubenrauch C. The molecular organogel n-decane/ 12-hydroxyoctadecanoic acid: sol–gel transition, rheology, and microstructure. Colloid Surface Physicochem Eng Aspect 2015;469:315–25.
66. Szczytko J, Vaupotic N, Osipov MA, Madrak K, Gorecka E. Effect of dimerization on the field-induced birefringence in ferrofluids. Phys Rev E 2013;87:062322.
67. Jordan PC. Field dependent chain formation by ferromagnetic colloids. Mol Phys 1979;38:769–80.
68. Kantorovich S, Ivanov AO, Rovigatti L, Tavares JM, Sciortino F. Nonmonotonic magnetic susceptibility of dipolar hard-spheres at low temperature and density. Phys Rev Lett 2013;110: 148306.
69. Osipov MA, Gorkunov MV. Effect of nanoparticle chain formation on dielectric anisotropy of nematic composites. Phys Rev E 2015;92:26.
70. Raşa M. Magnetic properties and magneto-birefringence of magnetic fluids. Eur. Phys. J. E 2000;2: 265–75.
71. Raşa M. Improved formulas for magneto-optical effects in ferrofluids. J Magn Magn Mater 1999; 201:170–3.
72. Janssen JJM, Perenboom JAAJ. Magneto-optical phenomena in magnetic fluids: the influence of orientation of anisotropic scatterers. J Magn Magn Mater 1989;81:14–24.
73. Pshenichnikov AF, Lebedev AV, Shliomis M. On the rotational effect in nonuniform magnetic fluids. Magnetohydrodynamics 2000;36:275–81.
74. Tsebers AO. Interfacial stresses in the hydrodynamics of liquids with internal rotations. Magnetohydrodynamics 1975;11:79–82.
75. Tsebers AO. Torques and hydrodynamics of a magnetic fluid in homogeneous rotating magnetic fields. Magnetohydrodynamics 1978;14:398–401.
76. Lebedev AV, Pshenichnikov AF. Motion of a magnetic fluid in a rotating magnetic field. Magnetohydrodynamics 1991;27:4–8.
77. Lebedev AV, Pschenichnikov AF. Rotational effect: the influence of free or solid moving boundaries. J Magn Magn Mater 1993;122:227–30.
78. Pshenichnikov AF, Lebedev AV. Action of a rotating magnetic field on a dielectric cylinder immersed in a magnetic fluid. J Appl Mech Tech Phys 1996;37:305–10.
79. Rosensweig RE, Popplewell J, Johnston RJ. Magnetic fluid motion in rotating field. J Magn Magn Mater 1990;85:171–80.
80. Bacri JC, Perzynski R, Shliomis MI, Burde GI. “Negative-Viscosity” effect in a magnetic fluid. Phys Rev Lett 1995;75:2128–31.

81. Sánchez JH, Rinaldi C. Magnetoviscosity of dilute magnetic fluids in oscillating and rotating magnetic fields. Phys Fluids 2010;22:043304–9.
82. Engel A, Müller H-W, Reimann P, Jung A. Ferrofluids as thermal ratchets. Phys Rev Lett 2003;91: 060602.
83. John T, Stannarius R. Experimental investigation of a brownian ratchet effect in ferrofluids. Phys Rev E 2009;80:050104.
84. Storozhenko AM, Stannarius R, Tantsyura AO, Shabanova IA. Measurement of the torque on diluted ferrofluid samples in rotating magnetic fields. J Magn Magn Mater 2017;431:66.
85. Usadel KD, Storozhenko A, Arefyev I, Nádasi H, Trittel T, Stannarius R, et al. Frequency-dependent conversion of the torque of a rotating magnetic field on a ferrofluid confined in a spherical cavity. Soft Matter 2019;15:9018.
86. Storozhenko A, Stannarius R, Eremin A, Aref'ev I. Torque on suspensions of anisotropic pigment particles and magnetic nanoparticles in a rotating magnetic field. Dresden: Poster at the 16th Ferrofluid Workshop; 2016.
87. May K, Eremin A, Stannarius R, Szabó B, Börzsönyi T, Appel I, et al. Exceptionally large magneto-optical response in dispersions of plate-like nanocrystallites and magnetic nanoparticles. J Magn Magn Mater 2017;431:79–83.